Research Journal in Civil, Industrial and Mechanical Engineering

DOI: 10.61424/rjcime
Journal Homepage: www.bluemarkpublishers.com/index.php/RJCIME

RJCIME
BLUEMARK PUBLISHERS

| RESEARCH ARTICLE

Innovative Thermo-Kinetic Approaches in Welding: The Impact on Microstructural Integrity of AISI 304L and AISI 316L Stainless Steels

Ochuko Goodluck Utu[1], Ifeanyichukwu Ugochukwu Onyenanu[2] ✉ and Ifunanya Mariagoretti Onyenanu[3]
[1]Department of Mechanical Engineering, Chukwuemeka Ojukwu Odumegwu University – Nigeria; Department of Welding and Fabrication Engineering Technology, Delta State Polytechnic Ogwashi Uku
[2]Department of Mechanical Engineering, Chukwuemeka Ojukwu Odumegwu University – Nigeria
[3]Department of Mechanical Engineering, Caritas University, Enugu – Nigeria
Corresponding Author: Ifeanyichukwu U. Onyenanu, **E-mail**: iu.onyenanu@coou.edu.ng

| ABSTRACT

AISI 304L and AISI 316L stainless steels, notable for their impressive corrosion resistance and mechanical attributes, find widespread application in the storage and transport of liquefied natural gas (LNG). Even so, these alloy types are susceptible to welding failure, a condition that involves the erosion of chromium at grain interfaces, which can weaken their overall structural soundness. This investigation explores novel thermo-kinetic methodologies aimed at mitigating weld decay in AISI 304L and AISI 316L weldments to prolong their operational lifespan in cryogenic settings. This investigation involved the development of 22 weldment test pieces employing tungsten inert gas (TIG) welding, succeeded by thermokinetic treatments at multiple temperatures (1050°C and 1150°C) for two-hour spans, and concluding with quenching in various substances: water, salt solution, and surrounding atmosphere. To evaluate alterations in microstructure and elemental content, the specimens underwent analysis via optical microscopy (OM), scanning electron microscopy (SEM), and energy-dispersive X-ray spectroscopy (EDX). Optical microscopy indicated that the control specimen exhibited a more irregular microstructure in contrast to those subjected to thermokinetic treatments, with the optimal temperature of 1112.68°C resulting in a smoother, more densely packed microstructure in samples cooled at room temperature. In contrast, samples that underwent water quenching followed by annealing exhibited coarse surface characteristics. EDX findings validated the existence of iron (Fe), chromium (Cr), and nickel (Ni) while also highlighting notable variations in corrosion potential seen across the samples, which spanned from -0.5 to 0.15 V about the Ag/AgCl electrode. Furthermore, wear analysis revealed a marginal increase in the coefficient of friction (CoF), stabilizing at 0.6 after 200 seconds, suggesting an enhancement in wear resistance at lower CoF values. This study underscores the benefits of TIG welding over shielded metal arc welding (SMAW) in mitigating weld decay, attributable to superior heat control and diminished hazardous emissions. The findings provide critical insights into the thermokinetic processing of AISI 304L and AISI 316L stainless steels, establishing fundamental parameters for augmenting their performance in rigorous applications.

| KEYWORDS

Thermo-Kinetic Approaches, Microstructural Integrity, AISI 304L Stainless Steel, AISI 316L Stainless Steel and Heat Treatment.

| ARTICLE INFORMATION

ACCEPTED: 07 November 2024 **PUBLISHED:** 11 December 2024 **DOI:** 10.61424/rjcime.v1.i1.162

1. Introduction

AISI 304L and AISI 316L types of stainless steels are extensively celebrated for their remarkable resistance to corrosion, mechanical qualities, and versatility, which makes them appropriate for various industrial applications, particularly in areas that need high reliability and safety, such as the oil and gas industry, food processing, and

chemical production (Utu et al., 2024). The primary constituents of these alloys include iron, chromium, and nickel, with AISI 304L exhibiting a reduced carbon content, thereby enhancing its corrosion resistance and weldability in comparison to standard 304 stainless steel (ASM International, 2020). AISI 316L, which is supplemented with molybdenum, offers even greater resistance to pitting and crevice corrosion, particularly in environments containing chloride ions (Callister & Rethwisch, 2020).

Although AISI 304L and AISI 316L possess beneficial qualities, the welding technique used with these materials can produce challenges, particularly weld decay, marked by the reduction of chromium at the boundaries of the weldment. This phenomenon substantially compromises the mechanical integrity and corrosion resistance of welded components, especially in hostile environments such as those encountered during the storage and transportation of liquefied natural gas (LNG) (Onyenanu et al., 2015; Utu et al., 2024). The chromium loss is a result of the high thermal input during the welding method, generating a heat-affected zone (HAZ) that unfavourably modifies the microstructural aspects (Li et al., 2022). Therefore, comprehending and managing weld decay is imperative for ensuring the durability and safety of stainless-steel structures.

Recent progress in welding technology has introduced pioneering thermo-kinetic methodologies that aim to alleviate the detrimental effects of welding on the microstructural integrity of stainless steel. Thermo-kinetic processing encompasses the manipulation of thermal cycles experienced by materials during welding, including the cooling rate and heat treatment, to optimize microstructural attributes and augment corrosion resistance (Zhao et al., 2021). Through meticulous control of parameters such as welding speed, heat input, and post-weld treatments, researchers have demonstrated encouraging outcomes in minimizing weld decay and enhancing the overall performance of welded joints. A study conducted by Utu et al. (2024) specifically investigates the optimization of thermo-kinetic techniques for regulating weld decay in AISI 304L and AISI 316L stainless steels. Their results indicate that the application of targeted heat treatment temperatures and quenching methodologies can significantly modify the microstructure, resulting in enhanced bonding and diminished susceptibility to corrosion. The research underscores the significance of selecting suitable quenching media and processing conditions, as these factors are crucial in attaining the desired mechanical properties and corrosion resistance.

However, despite the expanding corpus of research about thermo-kinetic methodologies, substantial gaps persist concerning the intricate mechanisms by which these approaches enhance weldment integrity in stainless steel. A majority of the existing studies emphasize generalized aspects of welding processes and their resultant effects, whereas a more comprehensive examination of the correlation between specific thermo-kinetic treatments and microstructural alterations is warranted (Zhang et al., 2023). Furthermore, the interaction between diverse alloy compositions and heat treatment parameters necessitates additional scrutiny to formulate customized solutions for various applications.

This investigation endeavours to address the discerned deficiencies in the existing research landscape by employing methodologically robust experimental frameworks to scrutinize the ramifications of avant-garde thermo-kinetic methodologies on the microstructural fidelity of AISI 304L and AISI 316L stainless steel alloys. Through a meticulous examination utilizing optical microscopy, scanning electron microscopy, and energy-dispersive X-ray spectroscopy, this inquiry elucidates the extent to which optimized thermal treatment and quenching protocols can augment performance metrics and mitigate weld degradation. The anticipated findings are poised to yield substantial revelations that may facilitate the advancement of welding methodologies and enhance material performance in high-stakes applications.

2. Literature Review

Weld decay, commonly denoted as intergranular corrosion, predominantly impacts stainless steels, particularly AISI 304L and AISI 316L, attributable to their vulnerability to chromium depletion at the grain boundaries during the welding process. This phenomenon transpires when the elevated temperatures associated with welding facilitate the diffusion of chromium away from the grain boundaries, culminating in a microstructural transformation that undermines corrosion resistance (Matsumoto et al., 2020). The depletion zone is typified by an insufficient presence

of chromium, which is critical for the development of a protective oxide layer, thereby rendering the material more susceptible to corrosion in hostile environments (Huang et al., 2021). Empirical studies have demonstrated that the severity of weld decay is modulated by various factors, encompassing the welding technique, thermal input, and cooling rate (Li et al., 2022). For example, investigations reveal that elevated heat inputs can intensify chromium depletion, leading to exacerbated intergranular corrosion (Zhang et al., 2023). Furthermore, the microstructural alterations that occur during welding, such as the emergence of sigma (σ) phase or carbides, additionally contribute to the deterioration of mechanical properties and corrosion resistance (Kumar et al., 2021). A range of strategies has been instituted to mitigate weld decay in stainless steel. A prevalent approach entails the optimization of welding parameters, inclusive of heat input and travel speed, to minimize the heat-affected zone (HAZ) (Chen et al., 2020). Diminishing the heat input can curtail the degree of chromium depletion, consequently augmenting the corrosion resistance of the weldment. An additional strategy encompasses post-weld heat treatment (PWHT), which aspires to reinstate the chromium content at the grain boundaries and alleviate residual stresses (Utu et al., 2024). Heat treatments, such as annealing, have been evidenced to enhance the microstructural stability of weldments by fostering the redistribution of chromium and other alloying constituents (Gao et al., 2021). Nonetheless, these methodologies frequently necessitate meticulous regulation of parameters to preempt the introduction of novel defects or alterations to the overall mechanical properties.

Thermo-kinetic approaches comprise a spectrum of methodologies aimed at regulating the thermal cycles experienced by materials throughout the welding process. These techniques incorporate heat treatment, cooling rates, and quenching methodologies, which are formulated to optimize the microstructural attributes of welded joints (Zhao et al., 2021). Heat treatment techniques, such as solution annealing and ageing, are particularly efficacious in enhancing the corrosion resistance of stainless steel by facilitating the establishment of a more homogeneous microstructure (Zhang et al., 2022). Moreover, the manipulation of cooling rates via diverse quenching media (e.g., water, oil, air) can markedly affect the resultant microstructure, influencing properties such as hardness, ductility, and tensile strength (Deng et al., 2023). The repercussions of thermo-kinetic approaches on microstructure and mechanical properties have been the subject of extensive investigation. For instance, research findings suggest that rapid cooling rates can engender the formation of martensitic structures, which enhance hardness but may concomitantly diminish ductility (Kumar et al., 2021). In contrast, more gradual cooling rates may facilitate the development of austenitic structures, which typically demonstrate superior ductility and corrosion resistance (Li et al., 2022).

Moreover, studies have demonstrated that optimized heat treatment can significantly improve the mechanical properties of welded joints by refining the grain structure and reducing the presence of detrimental phases (Gao et al., 2021). The use of response surface methodology (RSM) in optimizing these thermo-kinetic parameters has also been highlighted, providing a systematic approach to achieving desired outcomes in weldment performance (Utu et al., 2024).

2.1 Summary of Literature/ Research Gap

Notwithstanding the progress made in comprehending weld decay and the implementation of thermo-kinetic methodologies, notable constraints persist within the extant scholarly discourse. A considerable proportion of the prevailing literature is predominantly centred on broad welding methodologies and their implications for corrosion resistance, failing to thoroughly investigate the intricate mechanisms operative within AISI 304L and AISI 316L stainless steels (Huang et al., 2021). Furthermore, although a variety of strategies have been assessed to alleviate weld decay, there exists a deficiency of exhaustive studies that systematically scrutinize the interrelations among diverse thermo-kinetic treatments and their consequent effects on microstructural integrity. In light of the paramount significance of AISI 304L and AISI 316L in sectors necessitating superior corrosion resistance, an urgent requirement exists for targeted inquiries that examine the specific influences of pioneering thermo-kinetic approaches on these alloys. Research endeavours should aspire to elucidate the underlying mechanisms through which these treatments bolster microstructural integrity and delineate optimized parameters applicable in real-world welding contexts. This study aspires to bridge these gaps by examining the effects of regulated heat

treatment and quenching methodologies on the microstructural attributes and mechanical characteristics of AISI 304L and AISI 316L stainless steel alloys.

3. Methodology

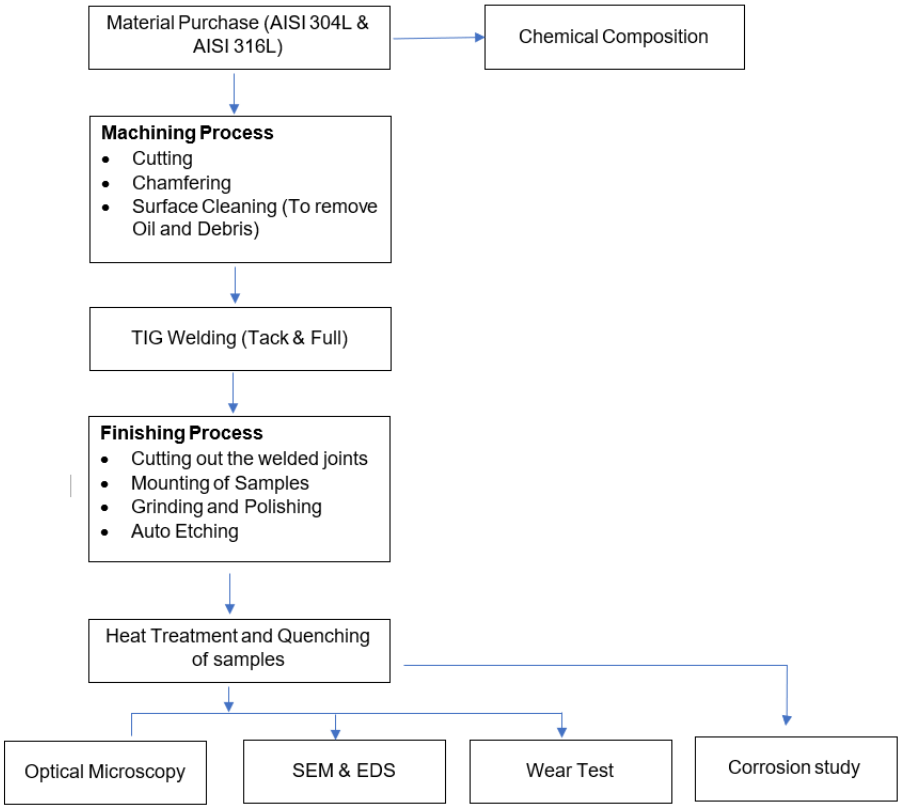

Figure 1: Detailed approach to the study

The schematics above (Figure 1) present a detailed pathway into the study. The samples were purchased from Turret Engineering Services, Port-Harcourt, Nigeria, who also provided the certificates of the materials, which contains the physical and chemical composition test results. This was confirmed using the PMI Oxford Instrument. The 304L and 316L flat bars were then cut to sizes at the Inspection and Testing Laboratory, Port-Harcourt, (Nig.) Ltd. The samples were now taken to the South African Institute of Welding Workshop (SAIW) for chamfering to have a root face of 1.6mm using the lathe. The new samples also underwent surface cleaning for oil removal and other debris before it was welded (first tacked and then fully welded) to have a single V-butt joint using the TIG welding process. The welded joints were now cut out (wire cutting) using the Electronic Discharge Machine (EDM) at the University of Johannesburg (DFC) workshop. The samples were then taken to the section lab, where they were mounted before grinding and polishing were done on the samples. This was followed by auto-etching the samples at the metallurgy laboratory. The samples were then subjected to heat treatment at three different temperatures (1050 ^{0}C, 1100^{0}C, 1150^{0}C) and various quenching mediums (Air, Water, salt, Salt + Annealing, Water + Annealing). After quenching, the samples were examined for chemical and morphological properties using Optical Microscopy (OM), Scanning Electron Microscopy (SEM), and Energy Dispersive Spectroscopy (EDS). Finally, the samples were also subjected to wear testing, and a corrosion study was also done on the samples in two different environments (Anodic and Cathodic).

3.1 Materials

The materials used for this study are the typical AISI type 304L and 316L stainless steel. Table 1 shows the nominal elemental compositions of typical AISI-type 304L and 316L stainless steel.

Table 1: Nominal chemical compositions of typical AISI type 304L and 316L stainless steel.

Element	AISI 304L Stainless Steel Material (% by wt.)	AISI 316L Stainless Steel Material (% by wt.)
Carbon (C)	0.03	0.03
Chromium (Cr)	19.0	16.50
Nickel (Ni)	10	11
Manganese (Mn)	2.00	2.00
Silicon (Si)	1.00	1.00
Molybdenum (Mo)	0.00	3.00
Phosphorus (P)	0.040	0.03
Sulphur (S)	0.035	0.035
Iron (Fe)	Remainder	Remainder

Source: (Tavares et al., 2010)

3.2 Sample Collection

The sample types AISI304L/316L stainless steel flat bar were purchased from Turret Engineering Services Port-Harcourt, Rivers State. The chemical composition of the materials was determined using PM/Oxford Instrument by Turret Engineering Services.

3.3 Sample Preparation

Each material type (AISI 3034L/ AISI 316L) flat bar was prepared by cutting into forty-four (44) pieces of 25mm x 25mm x 10mm. The cut pieces were paired into butt-weld single V-groove joints and welded by a tungsten inert gas (TIG) process. Twenty-two (22) welded pairs were produced. After the welding operation, the welded samples welded zone were cut off from the main material measuring 10mm x 10mm x 3mm. Depending on the availability of prequalified welders (skilled welders). The welders were tested/ prequalified on the American Welding Society (AWS) procedure. This is to eliminate limitations in workmanship. All welds were made with stainless steel (SS) filler rods containing carbon % by mass fraction compatible with that of base metal (0.028% for 304L and 0.031% for 316L). The weldment was free-air cooled. The welding procedure specification was referenced to AWS B2.1: Standard for welding procedure and performance Qualification, being one of the reference standards for welding procedure specifications. The welded samples used for the research work were chemically cleaned by immersions and in the process, the native oxides were removed. This native oxide is the initial oxide of Cr formed as a protective layer. These are considered to inhibit the diffusion of elements in the matrix. The heat input rate was determined before heating. All the welded specimens were prepared and thermo-kinetically treated (temperature input variable and quenching variable) in a furnace with a protective environment.

Figure 2: Clamps used to grip the sample, TIG Welding Machine, and Samples in Rectangular furnace Tray

3.4 Thermo-Kinetic Method

3.4.1 Heat Treatment Process

The welded austenitic stainless-steel grades 304 and 316 were initially prepared to standard dimensions (10 mm x 10 mm x 3 mm). The surfaces of these samples were polished to a mirror-like finish using silicon carbide abrasive papers ranging from 320 to 1200 grit, followed by diamond paste. The samples were then cleaned with ethanol and dried with warm air to remove any contaminants. The samples were divided into three main groups was heated to 1050 °C, and 1150 °C respectively. Heating was conducted in a muffle furnace with a controlled heating rate of 10°C per minute. Once the target temperature was reached, the samples were held at this temperature for 1 hour to ensure uniform temperature distribution throughout the sample.

After soaking, the samples were subjected to different cooling/quenching methods as follows:

1. **Water Quenching**: The samples were rapidly quenched in water at room temperature.
2. **Salt Solution Quenching**: The samples were quenched in a saturated NaCl solution at room temperature.
3. **Air Cooling**: The samples were allowed to cool naturally in the air.
4. **Water Quenching + Annealing**: The samples were quenched in water and then annealed at 250°C for 1 hour, followed by air cooling.
5. **Salt Solution Quenching + Annealing**: The samples were quenched in salt solution and then annealed at 250°C for 1 hour, followed by air cooling.

Control samples, which were not subjected to any heat treatment, were also prepared for comparative analysis.

Figure 3: Water Quenching, Aqueos Solution Quenching and Air Cooling

3.4.2 Heat Treatment Procedure

All the welded specimens were prepared and thermo-kinetically heat-treated in a furnace as follows:

a) Temperature 1050 ℃ (5 Samples)

- heat was applied to the specimens to a temperature threshold of 1050℃, soaked for 2 hours at this temperature, followed by quenching in water.
- heat was applied to the specimens to a temperature threshold of 1050℃, soaked for 2 hours at this temperature, followed by aqueous salt solution quenching
- heat was applied to the specimens to a temperature threshold of 1050℃, soaked for 2 hours at this temperature, followed by air cooling.
- Carried out stress relief for samples (a) and (b) at 300 ℃. Soaked for 1 hour at this temperature, followed by air cooling.

b) Temperature 1150 ℃ (5 Samples)

- heat was applied to the specimens to a temperature threshold of 1150℃, soaked for 2 hours at this temperature, followed by flowing water quenching.
- heat was applied to the specimens to a temperature threshold of 1150℃, soaked for 2 hours at this temperature, followed by aqueous salt solution quenching.

- heat was applied to the specimens to a temperature threshold of 1150℃, soaked for 2 hours at this temperature, followed by air cooling.
- Carried out stress relief for samples (i) and (j) at 300 ℃. Soaked for 1 hour at this temperature, followed by air cooling.

Figure 4: Before Heating, Heating if Furnace, and After Heating

3.5 Microstructural Characterization Techniques

3.5.1 Optical Microscopy (OM)

Some of the samples after heat treatment were prepared according to standard procedures (Georgios et Al., 2016) and metallographically evaluated to study their resulting microstructures. The grinding of the samples was carried out with various emery papers ranging from (150-250 grits) of successively finer grades lubricated by a gentle flow of water. Polishing was carried out on a rotating wheel covered with a short-pile cloth impregnated with 1um diamond polish and then OPS (Oxide Polishing Suspensions) solutions to remove scratches and to produce a smooth and mirror-like surface to observe the surface morphology. Etching, which helps to reveal grain boundaries and microstructure of the samples was done with hydrochloric acid. An optical metallurgical microscope fitted with a photographic device and computer fixture was then used to examine the surfaces of the samples. Various magnifications of X200, X400, X500, and X1000 were used to evaluate the microstructure. The metallographic examination of the solution annealing heat treatment stages 1, 2, and 3 was carried out at the metallography laboratory, university of Johannesburg, South Africa.

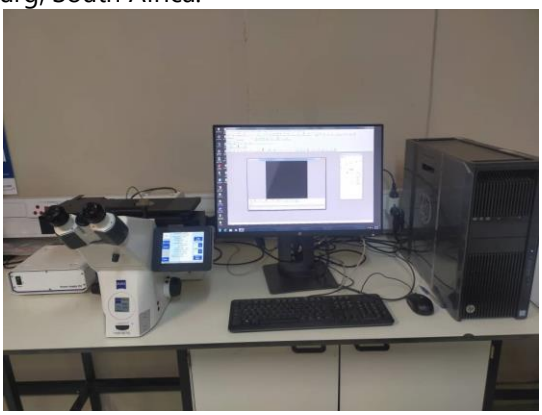

Figure 5: Optical Microscope

3.5.2 Scanning Selection Microscopy &EDS

Microstructural analysis began with the metallographic preparation of the samples. The samples were mounted in epoxy resin to facilitate handling and protect the edges. The mounted samples were then ground using silicon carbide abrasive papers, progressing from 320 grit to 1200 grit, to ensure a flat and scratch-free surface. After grinding, the samples were polished using a series of diamond suspensions (6 µm, 3 µm, and 1 µm) to achieve a mirror-like finish. Finally, the samples were etched using 10% oxalic acid to reveal the grain structure. Optical microscopy was initially employed to examine the microstructure and capture images of the grain structure. For more detailed microstructural characterization, Scanning Electron Microscopy (SEM) was used, providing high-

resolution images of the microstructural features such as grain boundaries, phase distribution, and any potential precipitates. Additionally, Energy Dispersive X-ray Spectroscopy (EDS) was performed in conjunction with SEM to determine the elemental composition of different regions within the samples, identifying any compositional changes due to the various heat treatments.

Figure 6: SEM/EDX Machine

4. Results and Discussion

4.1 Optical Microscopy Analysis

Figure 4.1 illustrates the optical micrograph depicting the microstructure of 316L austenitic stainless steel heated to 1050 ℃ at 10 magnification, serving as the reference sample in the study.

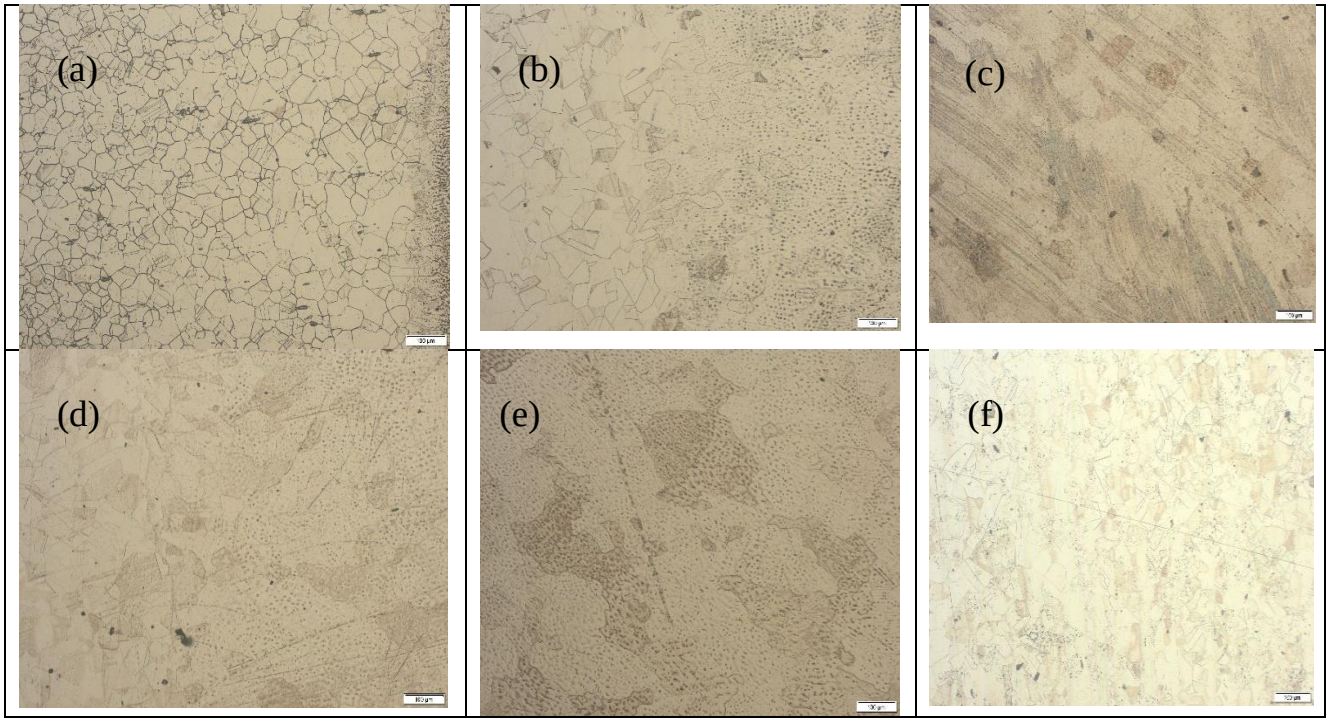

Figure 7: Optical microscopy results for 316L austenitic stainless steel 1050 ℃ (a) control sample (b) salt quenched (c) water quenched (d) air-cooled (e) salt quenched followed by annealing (f) water quenched followed by annealing.

Upon closer examination of the images, it can be observed that the control sample appears to exhibit a non-uniform distribution of particles, suggesting inadequate bonding or packing. However, following the application of heat treatment at 1050℃ and subsequent quenching using various quenching media, the results obtained indicate a more homogeneously distributed matrix with improved bonding characteristics. Specifically, sample (e), which underwent quenching in salt following annealing, displayed a notably smoother surface, indicating a more secure bonding of particles. In contrast, the air-cooled sample (d) exhibited closely packed particles that closely resembled the surface morphology of sample (e). Sample (b) demonstrated partial bonding and was found to be most similar to the control sample (a). Notably, sample (b) was subjected to salt quenching without prior annealing, highlighting the distinct effects of different processing conditions on the bonding characteristics of the samples. Overall, the results suggest that the control sample (a) retained a bonding structure similar to the original material. The pictures were taken at the heat-affected zones (HAZ).

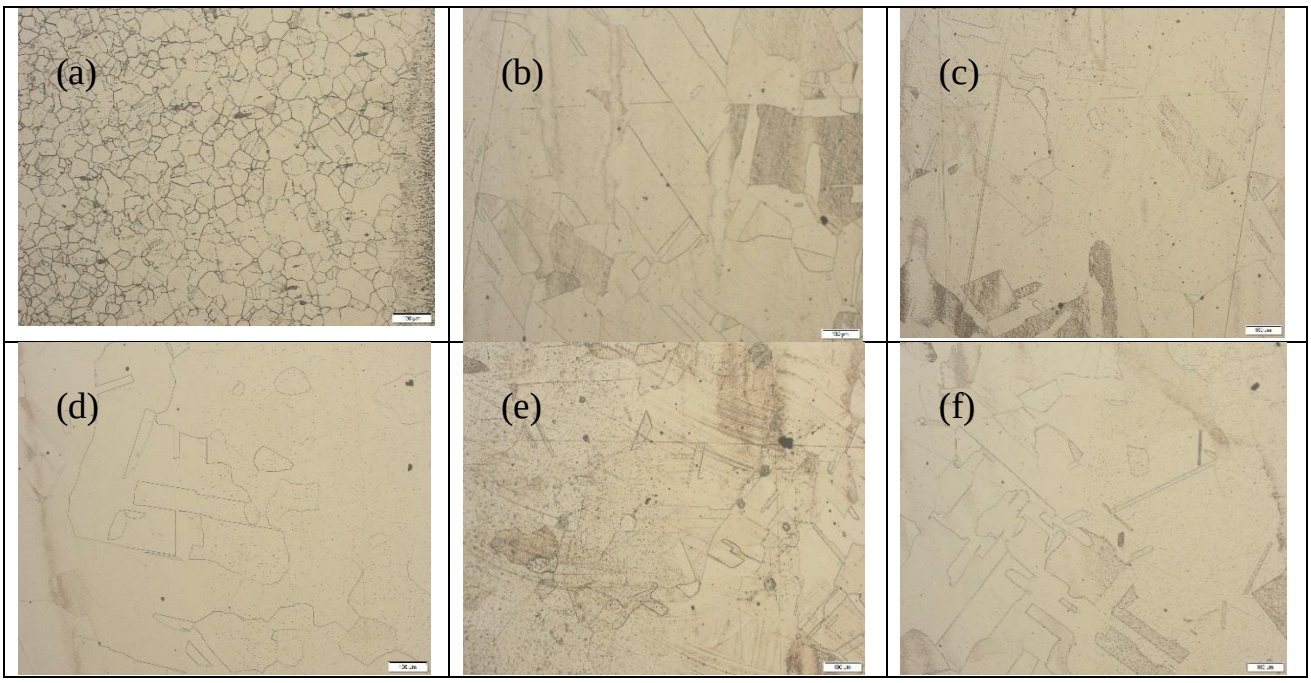

Figure 8: Optical microscopy results for 316L austenitic stainless steel 1150 ℃ (a) control sample (b) salt quenched (c) water quenched (d) air-cooled (e) salt quenched followed by annealing (f) water quenched followed by annealing.

Figure 8 depicts the optical micrograph illustrating the microstructure of 316L austenitic stainless steel when exposed to a temperature of 1150 ℃ at 10 magnification, serving as the reference specimen in the research. Upon careful examination of the images, it is apparent that the control specimen seems to display an uneven distribution of particles, indicating possible deficiencies in bonding or packing. However, after subjecting the material to heat treatment at 1150℃ followed by quenching using various media, the findings suggest a more evenly distributed matrix with enhanced bonding properties. Specifically, specimen (d), which was cooled by air, exhibited a significantly smoother surface, implying a more secure bond between particles. Furthermore, the water-quenched specimen (f), following annealing, showed densely packed particles closely resembling the surface characteristics of the specimen (d). Specimens (b) and (e) displayed partial bonding and resembled the control specimen (a) the most, which had coarse surfaces. Remarkably, specimen (c) underwent salt quenching without prior annealing, revealing the distinct impacts of different processing conditions on the bonding properties of the specimens, demonstrating significant differences from (b) to itself. Overall, the outcomes suggest that the control specimen (a) maintained a bonding structure akin to the original material. The images were captured at the heat-affected zones (HAZ).

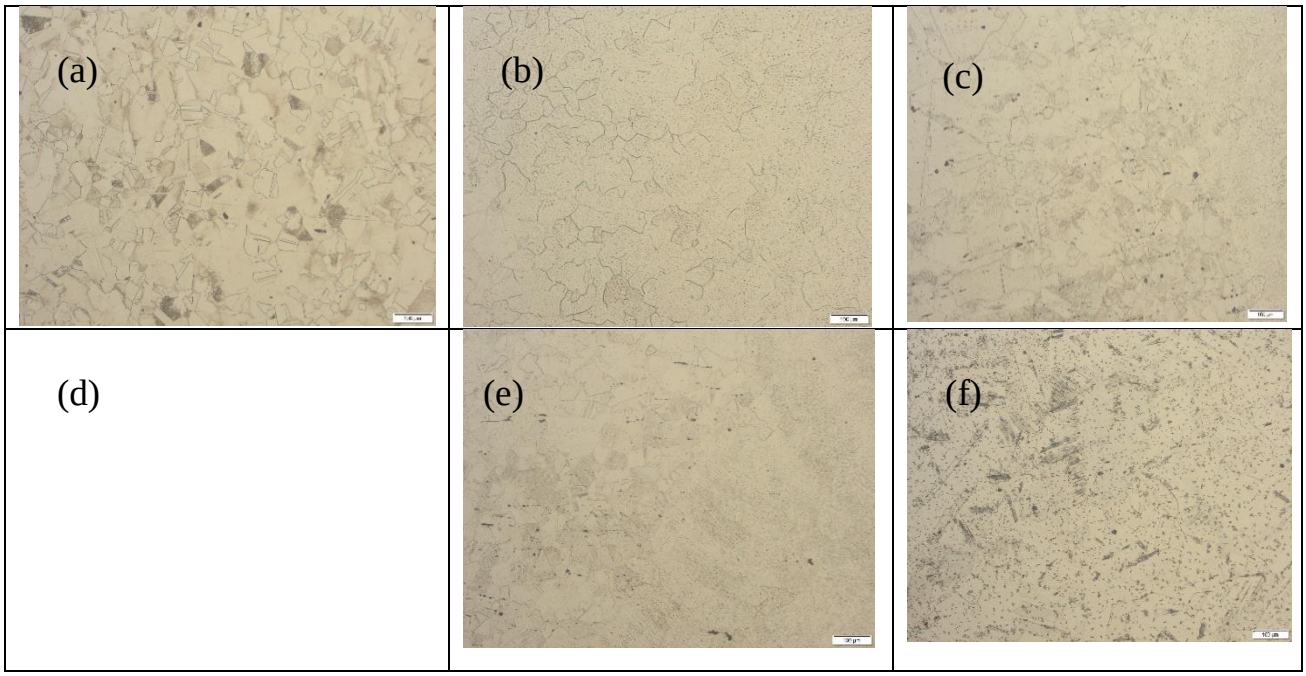

Figure 9: Optical microscopy results for 304L austenitic stainless steel 1050 ℃ (a) control sample (b) salt quenched (c) water quenched (d) air-cooled (e) salt quenched followed by annealing (f) water quenched followed by annealing.

Figure 9 illustrates the optical micrograph displaying the microstructure of 304L austenitic stainless steel after exposure to a temperature of 1050 ℃ at 10x magnification, serving as the reference specimen in the study. Upon meticulous examination of the images, it is evident that the control specimen exhibits an irregular distribution of particles, suggesting potential deficiencies in bonding or packing. Nevertheless, subsequent heat treatment at 1050℃ followed by quenching using different media resulted in a more uniformly distributed matrix with improved bonding characteristics. Specifically, specimen (e), which underwent salt quenching post-annealing, displayed a notably smoother surface, indicating a more robust bond between particles. Additionally, the water-quenched specimen (f), post-annealing, exhibited densely packed particles closely resembling the surface features of the sample (a); these two samples have similar surfaces, but they lack the strong bonding observed in the other specimens, implying a coarser nature. Samples (c) and (e) share similarities as they represent the finest samples in the results, showcasing smooth and even bonding, while also noting that sample (b) does not exhibit as uniform bonding as (e). Interestingly, sample (c) underwent salt quenching without prior annealing, highlighting the distinct effects of varying processing conditions on the bonding properties of the specimens, showcasing significant differences from (b) and (c) to itself. In general, the results indicate that the control specimen (a) preserved a bonding structure similar to the original material. The images were taken at the heat-affected zones (HAZ).

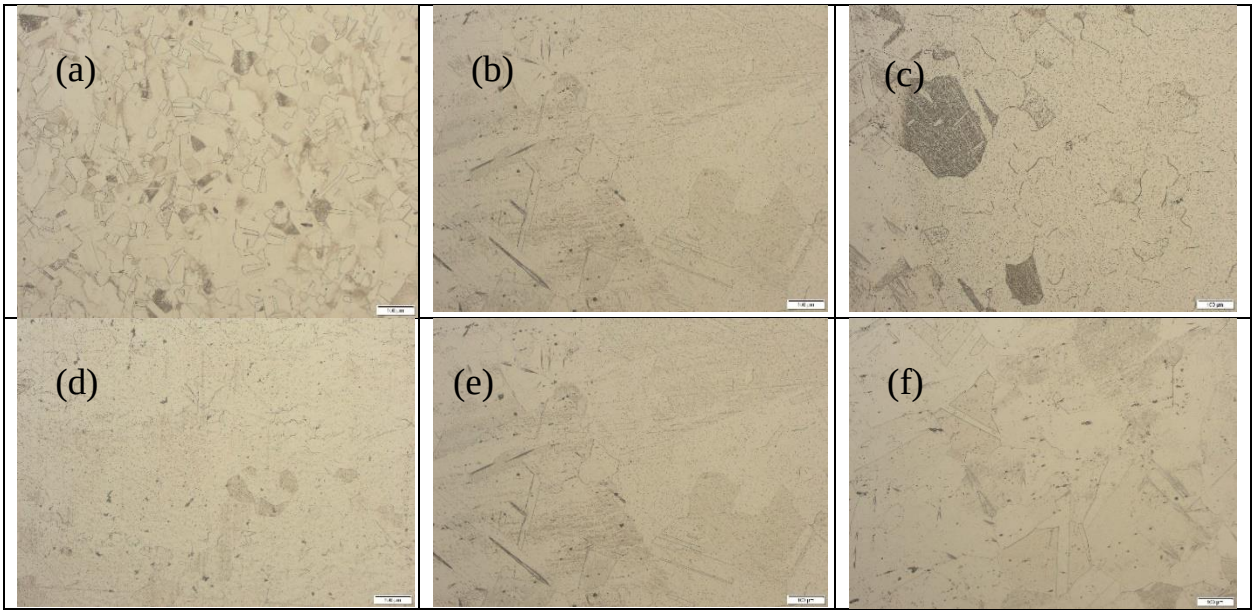

Figure 10: Optical microscopy results for 304L austenitic stainless steel 1150 ℃ (a) control sample (b) salt quenched (c) water quenched (d) air-cooled (e) salt quenched followed by annealing (f) water quenched followed by annealing

Figure 10 illustrates the optical micrograph portraying the microstructure of 304L austenitic stainless steel under exposure to a temperature of 1150 ℃ at 10x magnification, serving as the reference sample in the study. Upon meticulous examination of the images, it becomes evident that the control specimen exhibits an uneven distribution of particles, hinting at potential deficiencies in bonding or packing. Nevertheless, after subjecting the material to heat treatment at 1150℃ followed by quenching utilizing various media, the results indicate a more uniformly distributed matrix with improved bonding characteristics. Specifically, specimen (d), which was cooled by air, displayed a notably smoother surface, suggesting a more robust bond between particles. Moreover, the specimen quenched with water (f), post-annealing, displayed densely packed particles closely resembling the surface characteristics of samples (d) and (e), which exhibit almost identical surfaces showcasing a strong bond between them compared to other samples. These samples emerge as the most superior in terms of bonding, being smoothly and evenly bonded. It is also noted that sample (c) does not exhibit uniform bonding, as seen in sample (b). Interestingly, sample (c) underwent salt quenching without prior annealing, highlighting the distinct effects of varied processing conditions on the bonding properties of the specimens, showcasing significant differences from (c) to (b) itself. Overall, the results indicate that the control sample (a) preserved a bonding structure similar to the original material. The images were captured at the heat-affected zones (HAZ). Refer to Appendix B1 for the results obtained for the parent material (PM) and the welded joints (WJ).

4.2 Scanning Electron Microscopy and EDX

Scanning electron microscopy (SEM) was utilized to analyze the surface morphology of the (WJ, HAZ, and PM) welded joint, heat affected area, and the parent materials.

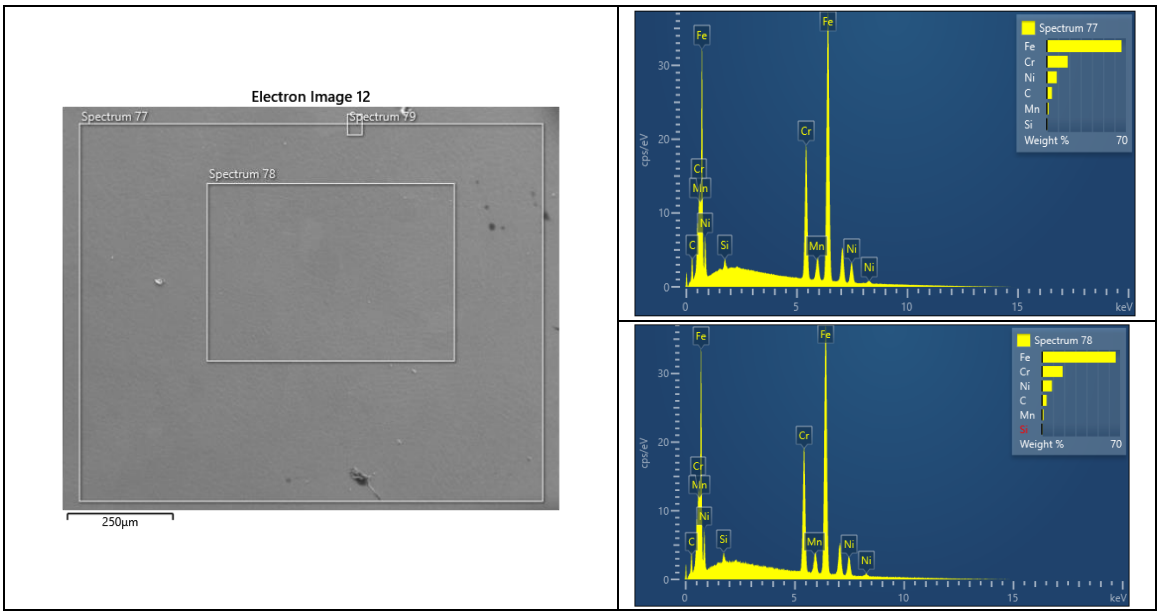

Figure 11: SEM result and EDX analysis of 304L stainless heat treated at 1050℃ and quenched in water.

Figure 11a shows the high-resolution SEM image captured at a magnification of 250x with a scale bar representing 1µm; this image allows the observation of the nanoscale features; the image reveals a relatively smooth surface with evenly dispersed particles after heat treatment, the presence of uniformly dispersed particles of the materials after welding/heat treatment. While the EDS result summarizes the elements detected in sample 3(d). Figure 11b shows peaks at 34 Cps/eV,16 Cps/eV, and 9 Cps/eV corresponding to Iron (Fe), Chromium (Cr), and Nickel (Ni) respectively. The peak intensities suggest that (Fe) Iron is the most abundant element in the sample, followed by chromium (Cr) and Nickel (Ni).

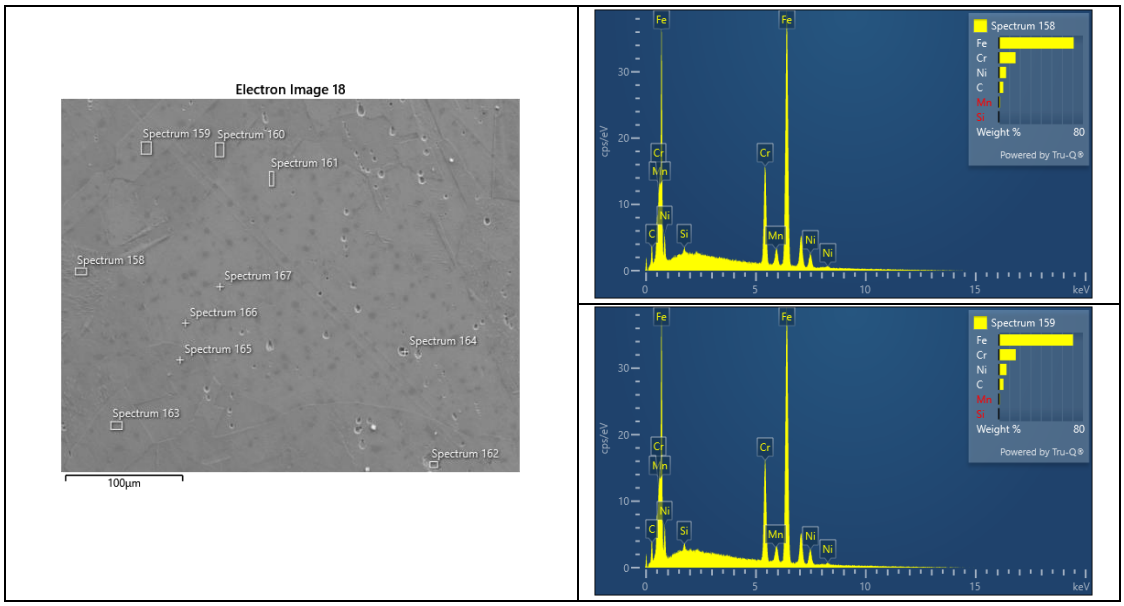

Figure 12: SEM result and EDX analysis of 304L stainless heat treated at 1050℃ and quenched in salt

Figure 12a depicts the high-resolution scanning electron microscope (SEM) image obtained at a magnification of 250x, accompanied by a scale bar denoting 1µm. This image facilitates the examination of the nanoscale characteristics, revealing a surface that is a bit coarse, and particles are not evenly distributed after the application of heat. The image illustrates the presence of particles uniformly dispersed in the material following the welding or heat treatment process. Meanwhile, the Energy Dispersive X-ray Spectroscopy (EDS) analysis provides a summary of

the elements identified in sample 4. In Figure 12b, peaks are observed at 34 Cps/eV, 16 Cps/eV, and 9 Cps/eV, corresponding to Iron (Fe), Chromium (Cr), and Nickel (Ni) respectively. The intensities of these peaks imply that Iron (Fe) is the most prevalent element in the sample, with Chromium (Cr) and Nickel (Ni) following suit.

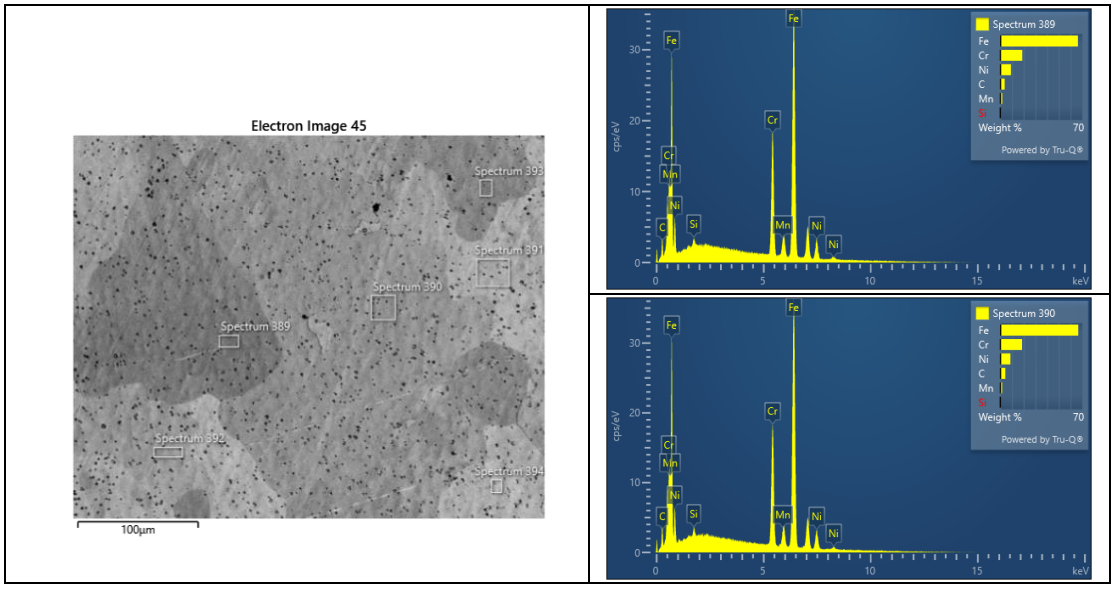

Figure 13: SEM result and EDX analysis of 304L stainless heat treated at 1050°C and annealed in water.

Figure 13a illustrates the high-resolution scanning electron microscope (SEM) image acquired at a magnification of 250x, accompanied by a scale bar indicating 1µm. This depiction enables the analysis of nano-scale characteristics, unveiling a somewhat rough surface with particles exhibiting non-uniform distribution post-heat application. The visualization demonstrates the homogeneous dispersion of particles within the material after welding or heat treatment. Concurrently, the Energy Dispersive X-ray Spectroscopy (EDS) examination offers a concise overview of the elements detected in sample 27. In Figure 13b, peaks are identified at 34 Cps/eV, 16 Cps/eV, and 9 Cps/eV, corresponding to Iron (Fe), Chromium (Cr), and Nickel (Ni) respectively. The magnitudes of these peaks suggest that Iron (Fe) predominates as the elemental constituent in the sample, with Chromium (Cr) and Nickel (Ni) following in succession.

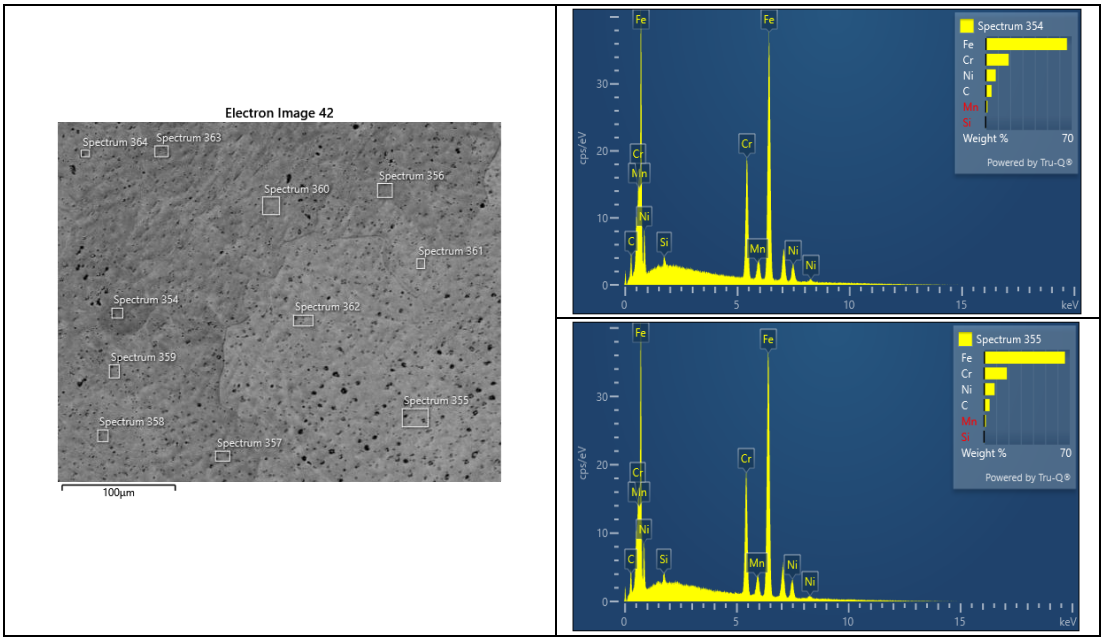

Figure 14: SEM result and EDX analysis of 304L stainless heat treated at 1050°C and annealed in salt.

The high-resolution SEM image in Figure 14a, captured at 250x magnification and featuring a 1µm scale bar, facilitates the examination of nanoscale properties, revealing a coarse surface with uneven particle distribution after heating. Post-welding, particles are uniformly dispersed. EDS analysis provides a summary of the elements in sample 29, with Figure 14b showing peaks at 34, 16, and 9 Cps/eV for Iron, Chromium, and Nickel, indicating Iron's prevalence, followed by Chromium and Nickel.

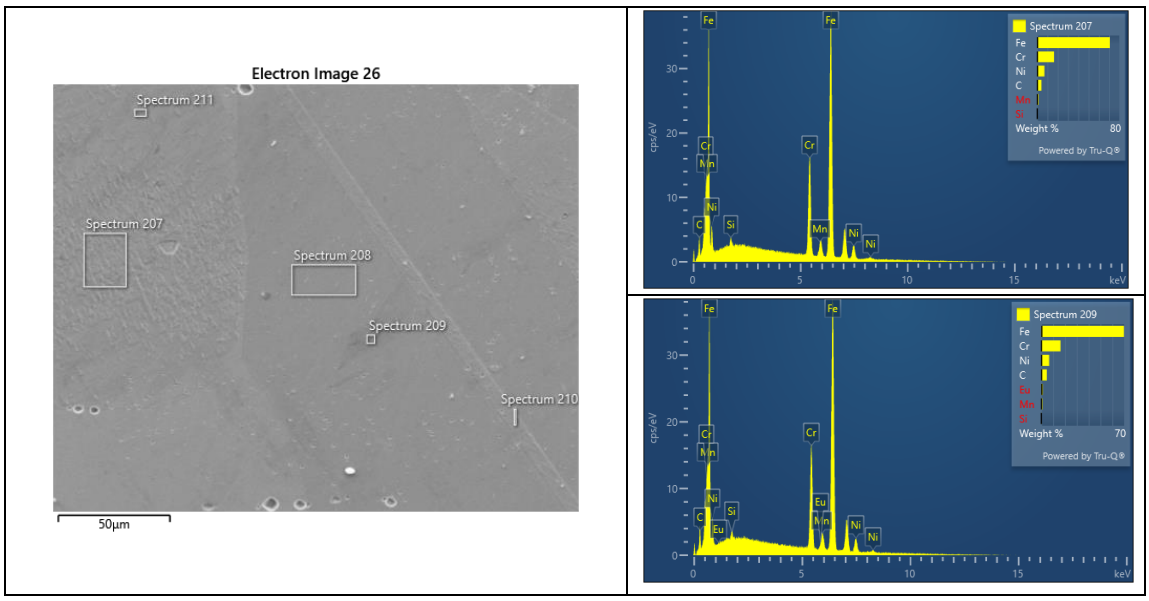

Figure 15: SEM result and EDX analysis of 304L stainless heat treated at 1150℃ and Air cooled

Figure 15a illustrates a high-resolution SEM image at 250x magnification, accompanied by a 1µm scale bar, enabling nanoscale analysis. The image shows a coarse surface with uneven particle distribution post-heat application. Following welding, particles are evenly spread. EDS analysis identifies elements in sample 13, with Figure 15b displaying peaks at 34, 16, and 9 Cps/eV for Fe, Cr, and Ni, suggesting Iron's predominance, followed by Chromium and Nickel.

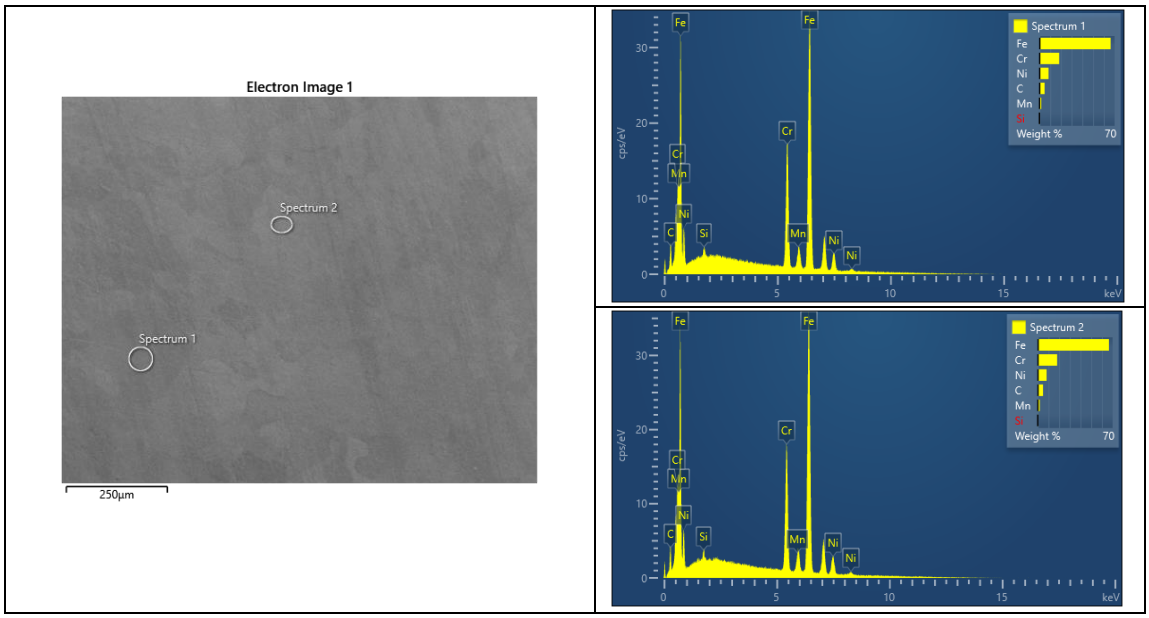

Figure 16: SEM result and EDX analysis of 304L stainless heat treated at 1150℃ and annealed with water

Figure 16a depicts the high-resolution scanning electron microscope (SEM) image obtained at a magnification of 250x, accompanied by a scale bar denoting 1µm. This image facilitates the examination of the nanoscale characteristics, revealing a notably smooth surface, with particles evenly distributed after the application of heat. The image illustrates the presence of particles uniformly dispersed in the material following the welding or heat treatment process. Meanwhile, the Energy Dispersive X-ray Spectroscopy (EDS) analysis provides a summary of the elements identified in sample 10. In Figure 16b, peaks are observed at 34 Cps/eV, 16 Cps/eV, and 9 Cps/eV, corresponding to Iron (Fe), Chromium (Cr), and Nickel (Ni) respectively. The intensities of these peaks imply that Iron (Fe) is the most prevalent element in the sample, with Chromium (Cr) and Nickel (Ni) following suit.

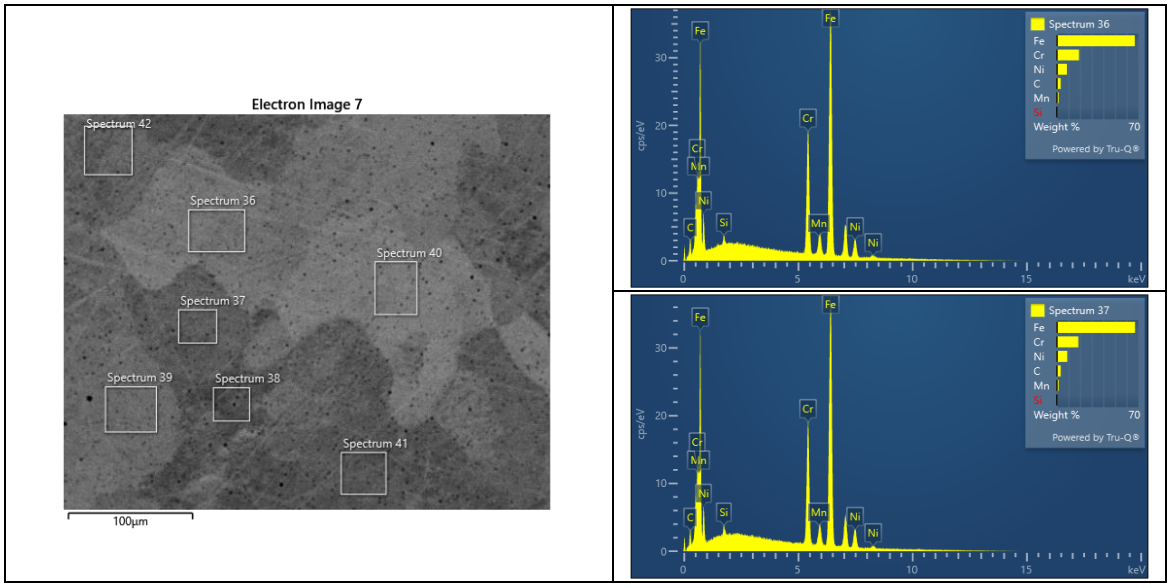

Figure 4.17: SEM result and EDX analysis of 304L stainless heat treated at 1150℃ and annealed with salt

In Figure 4.17a, a high-resolution SEM image at 250x magnification, with a 1µm scale bar, is presented to examine nanoscale features. The image reveals a coarse surface with uneven particle distribution after heating. Post-welding, particles are uniformly distributed. EDS analysis for sample 11 is summarized, showing peaks at 34, 16, and 9 Cps/eV for Fe, Cr, and Ni in Figure 17b, indicating Iron's dominance, followed by Chromium and Nickel.

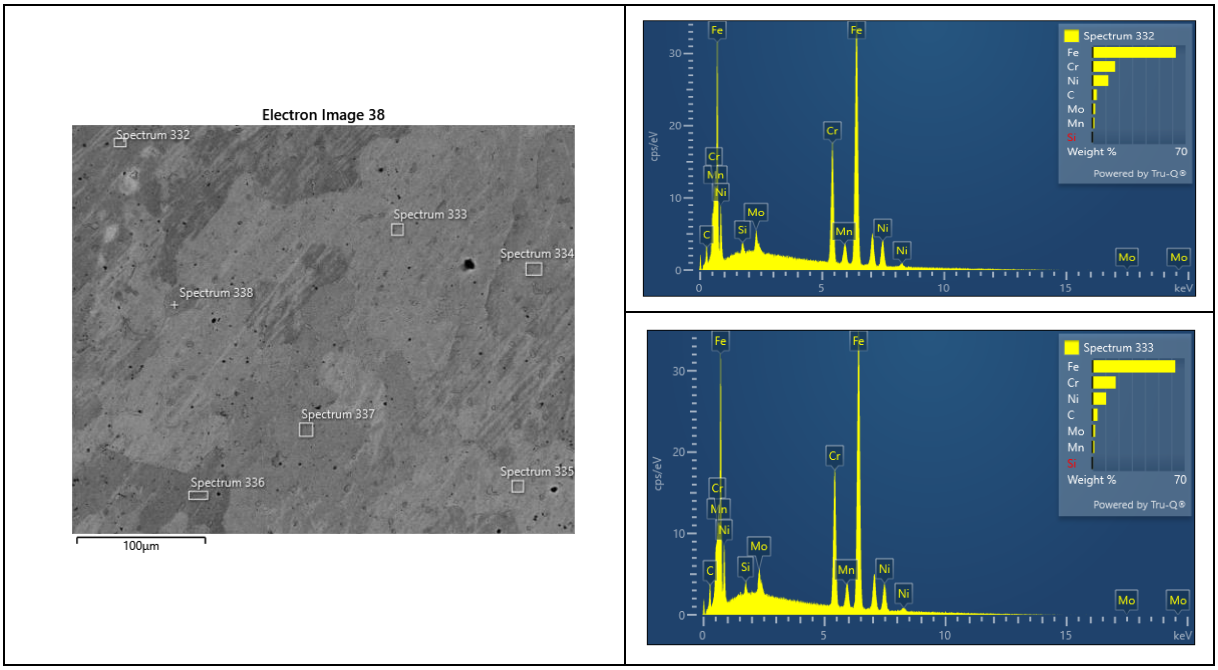

Figure 4.18: SEM result and EDX analysis of 316L stainless heat treated at 1050℃ and quenched in water.

The SEM image in Figure 4.18a, taken at 250x magnification and including a 1µm scale bar, allows for detailed nanoscale examination, revealing a coarse surface with particles unevenly distributed post-heat treatment. After welding, particles are uniformly dispersed. EDS analysis of sample 5 shows peaks at 34, 16, and 9 Cps/eV for Iron, Chromium, and Nickel in Figure 18b, suggesting Iron's prevalence, followed by Chromium and Nickel.

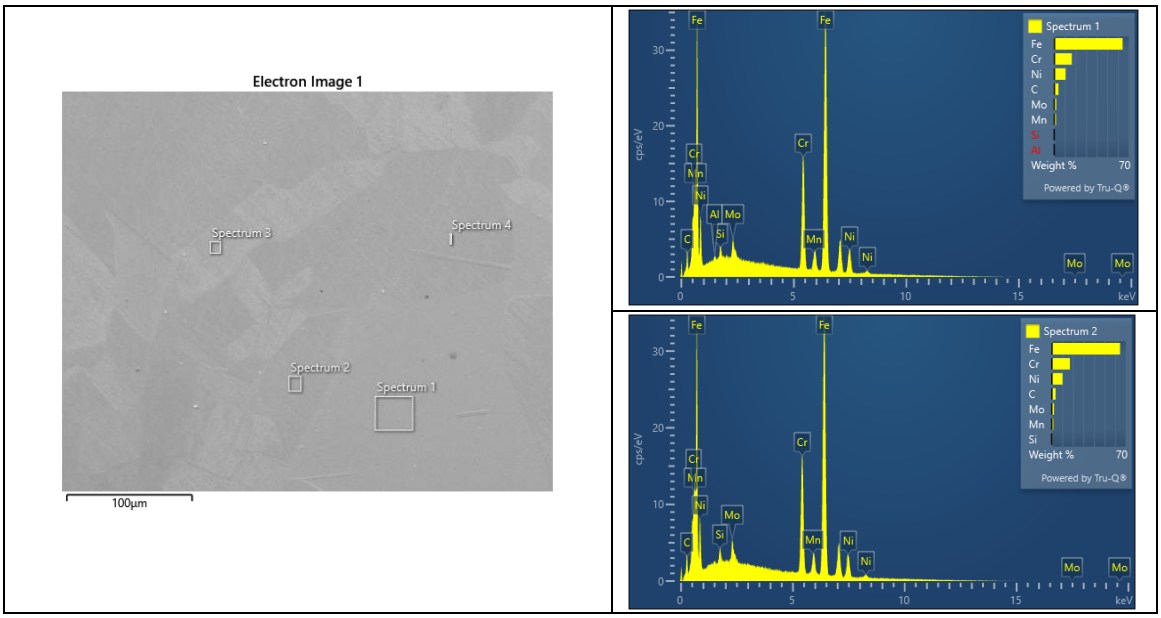

Figure 4.19: SEM result and EDX analysis of 316L stainless heat treated at 1050℃ and air-cooled

Figure 4.19a displays a high-resolution SEM image at 250x magnification, featuring a 1µm scale bar. The image aids in examining nanoscale characteristics, showing a coarse surface with uneven particle distribution after heating. Post-welding, particles are evenly dispersed. EDS analysis provides element identification for sample 1, with Figure 4.19b showing peaks at 34, 16, and 9 Cps/eV for Fe, Cr, and Ni, indicating Iron's dominance, followed by Chromium and Nickel.

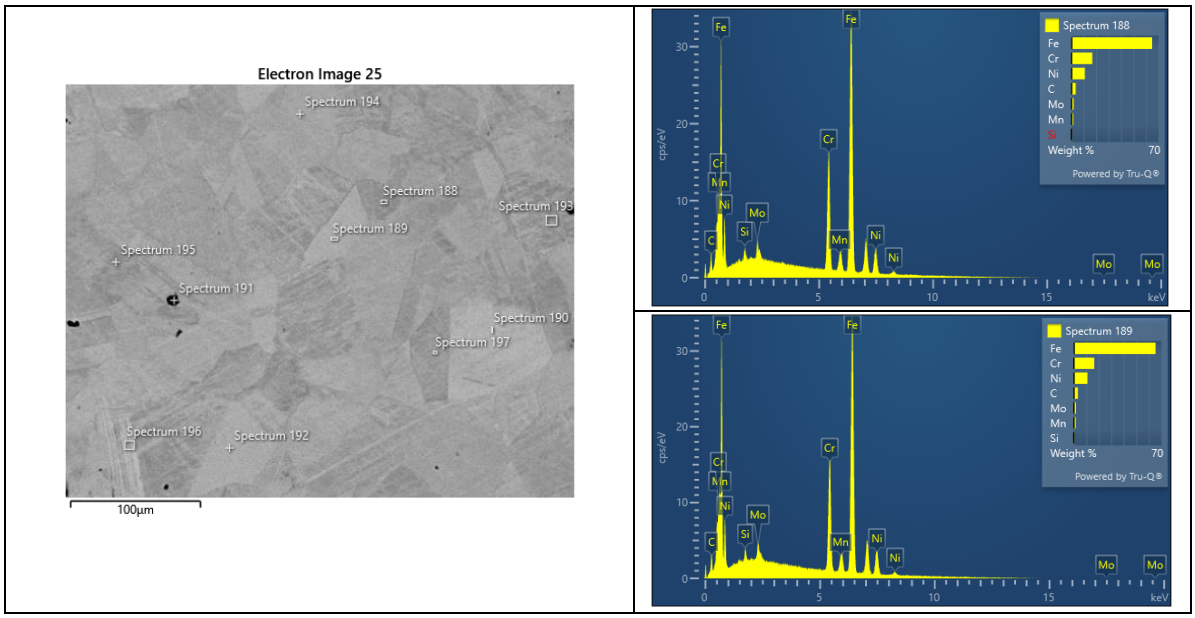

Figure 20: SEM result and EDX analysis of 316L stainless heat treated at 1050℃ and salt quenched

In Figure 20a, a 250x magnified high-resolution SEM image is shown with a 1µm scale bar, aiding in examining nanoscale characteristics. The image reveals a coarse surface with uneven particle distribution post-heating. Post-welding, particles are uniformly dispersed. EDS analysis of sample 2 identifies elements, with Figure 20b displaying peaks at 34, 16, and 9 Cps/eV for Iron, Chromium, and Nickel, suggesting Iron is the most prevalent, followed by Chromium and Nickel.

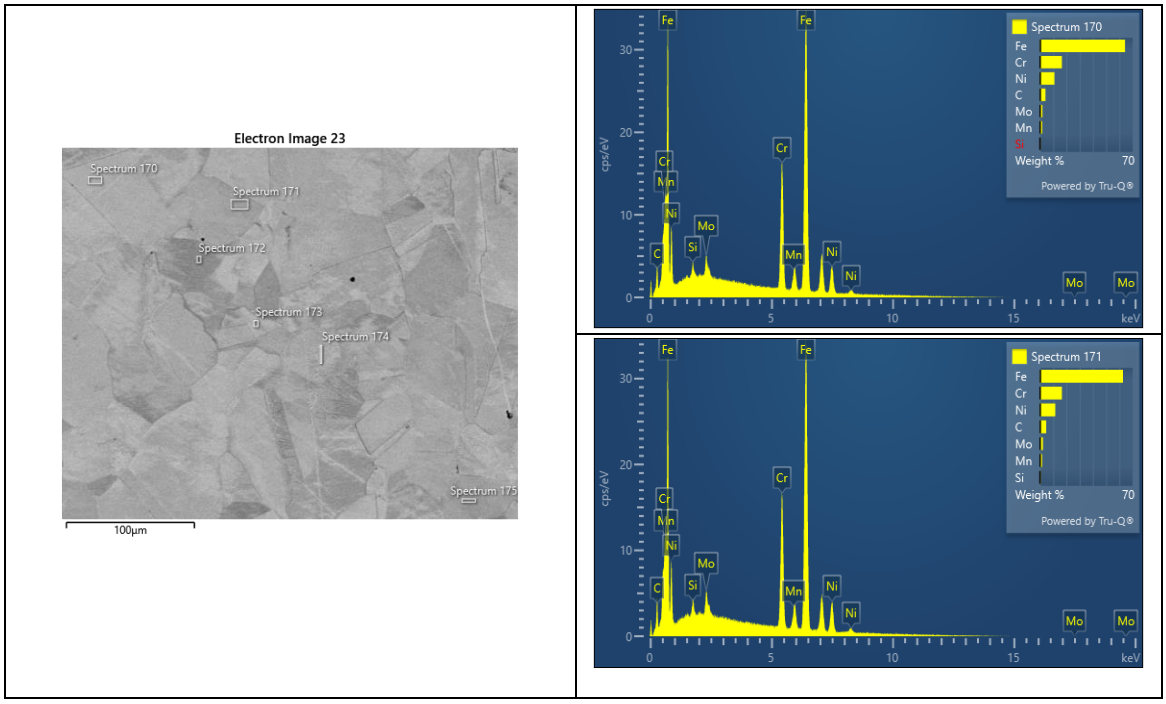

Figure 21: SEM result and EDX analysis of 316L stainless heat treated at 1050℃ and annealed in salt

The high-resolution SEM image in Figure 21a, taken at 250x magnification and marked with a 1µm scale bar, facilitates nanoscale feature analysis, revealing a somewhat coarse surface with uneven particle distribution post-heat application. After welding, particles appear uniformly dispersed. EDS analysis of sample 31 is summarized, with Figure 21b showing peaks at 34, 16, and 9 Cps/eV for Fe, Cr, and Ni, indicating Iron's predominance, followed by Chromium and Nickel.

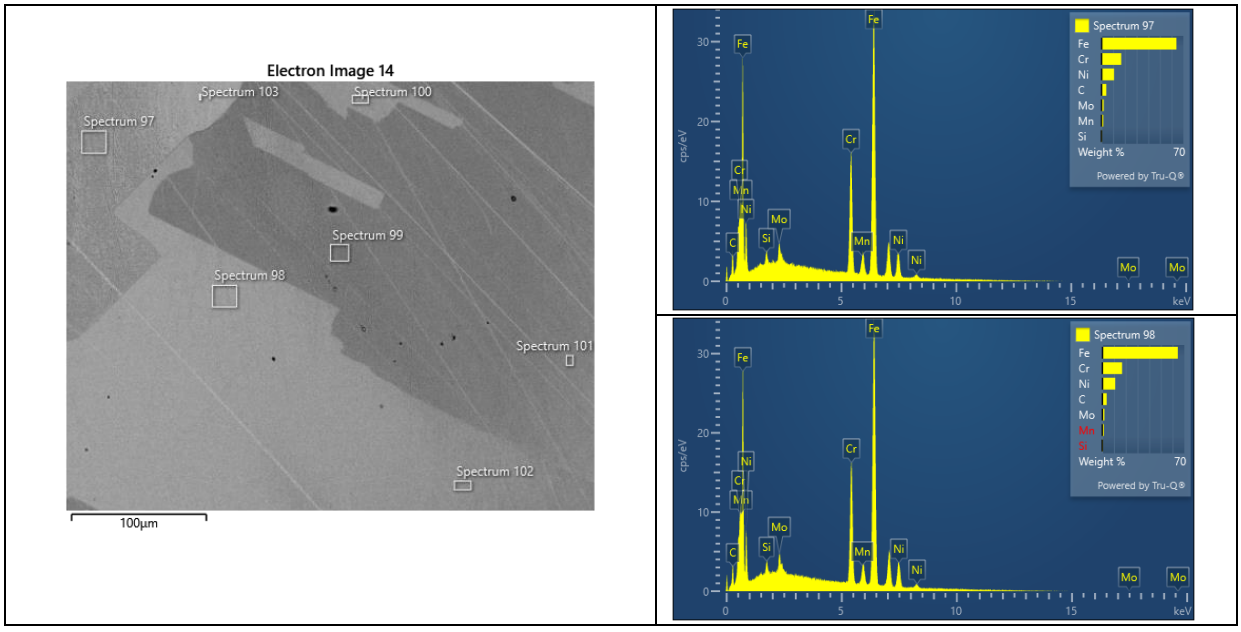

Figure 22: SEM result and EDX analysis of 316L stainless heat treated at 1150℃ and Air cooled

Figure 22a presents a high-resolution SEM image captured at 250x magnification, including a 1µm scale bar. This image aids in studying nanoscale properties, revealing a slightly coarse surface with particles unevenly distributed after heating. Following welding or heat treatment, the material shows uniformly dispersed particles. The EDS analysis outlines the elements found in sample 14, with Figure 22b showing peaks at 34, 16, and 9 Cps/eV for Iron, Chromium, and Nickel, indicating Iron as the most common element, with Chromium and Nickel also present.

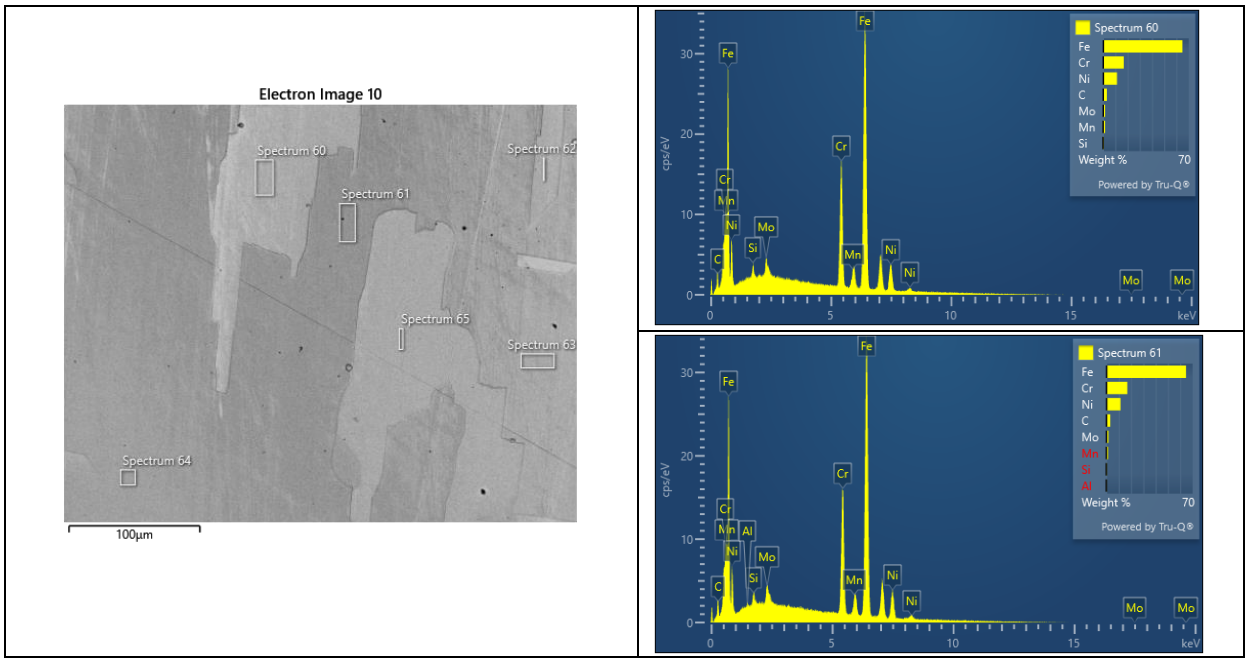

Figure 23: SEM result and EDX analysis of 316L stainless heat treated at 1150℃ and salt quenched

In Figure 23a, a high-resolution SEM image at 250x magnification is depicted, along with a 1µm scale bar. This image helps examine the nanoscale features, showing a coarse surface with uneven particle distribution after heat treatment. The welding process results in uniformly dispersed particles in the material. The EDS analysis identifies elements in sample 18, with Figure 23b displaying peaks at 34, 16, and 9 Cps/eV for Fe, Cr, and Ni. Iron is the most abundant element, followed by Chromium and Nickel.

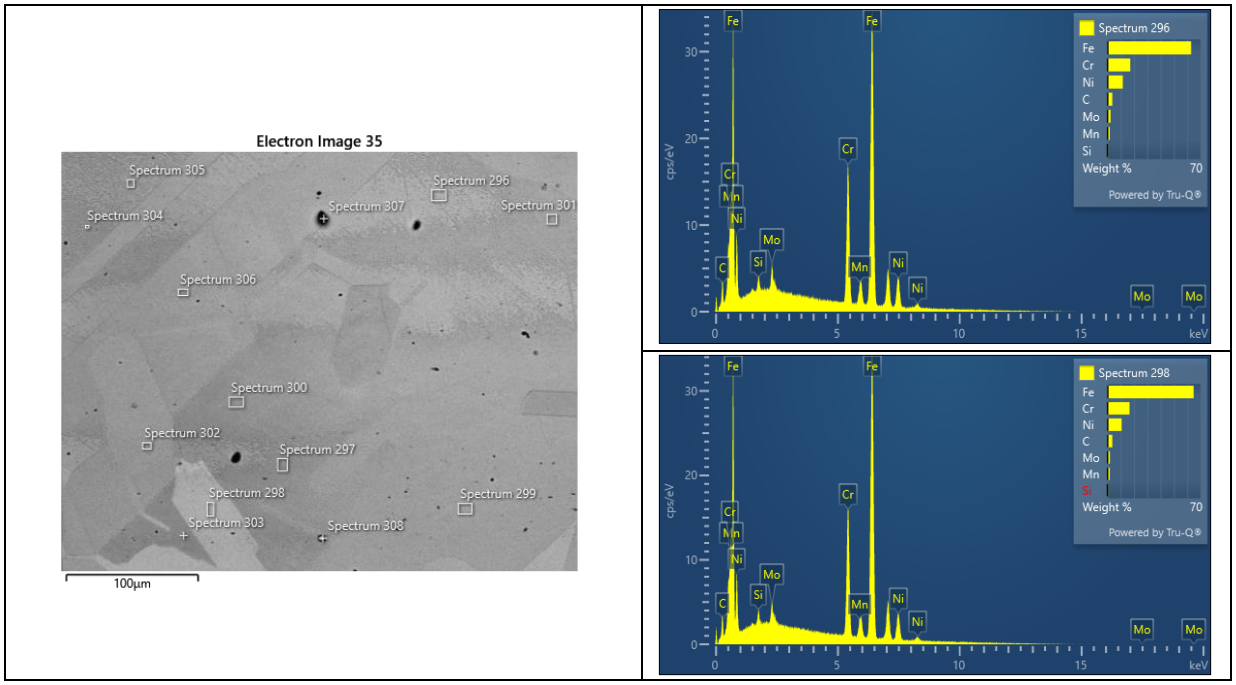

Figure 24: SEM result & EDX analysis of 316L stainless heat treated at 1150°C and quenched in water

Figure 24a showcases a high-resolution SEM image at 250x magnification, complete with a 1µm scale bar. The image allows for nanoscale analysis, revealing a somewhat coarse surface with uneven particle distribution after heat application. Post-welding or heat treatment, particles appear uniformly spread throughout the material. Concurrently, EDS analysis highlights the elements in sample 24. Figure 24b shows peaks at 34, 16, and 9 Cps/eV for Iron (Fe), Chromium (Cr), and Nickel (Ni), respectively. These peaks suggest Iron is the predominant element, followed by Chromium and Nickel.

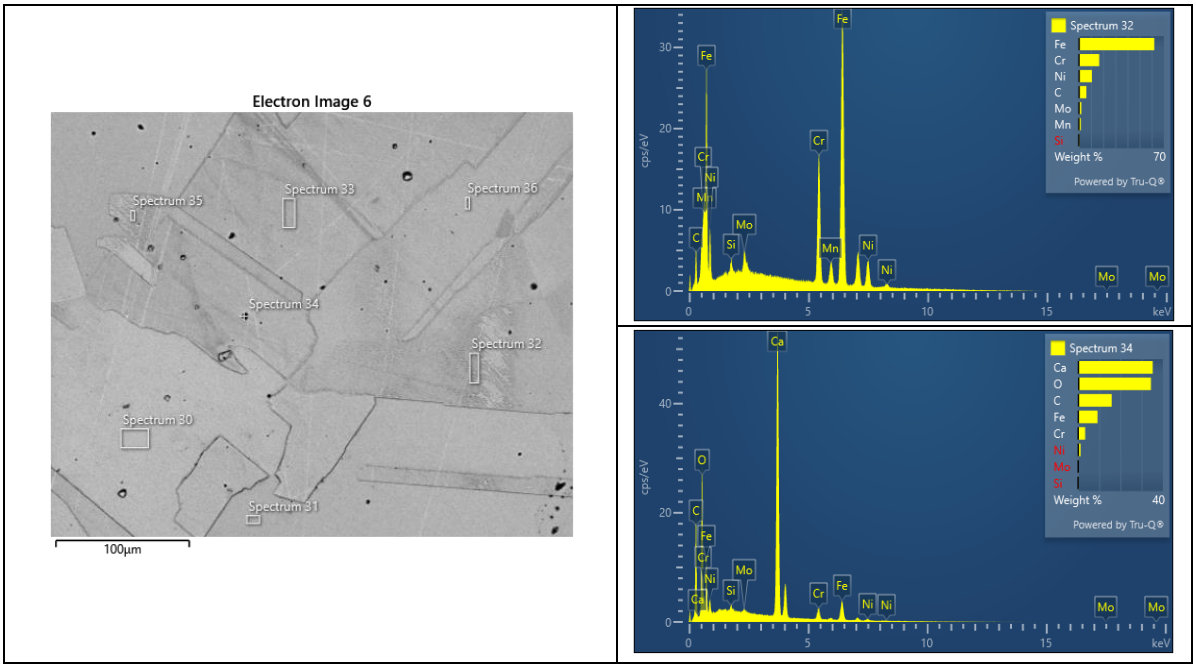

Figure 25: SEM result and EDX analysis of 316L stainless heat treated at 1150°C and quenched in salt

The SEM image in Figure 25a, captured at 250x magnification with a 1µm scale bar, facilitates nanoscale property examination, showing a coarse surface and uneven particle distribution after heating. Post-welding, particles are

uniformly spread. EDS analysis of sample 18, shown in Figure 25b, identifies peaks at 34, 16, and 9 Cps/eV for Iron, Chromium, and Nickel, with Iron being the most abundant element.

5. Discussion

The findings derived from the exploration of innovative thermo-kinetic methodologies in welding, particularly concerning AISI 304L and AISI 316L stainless steel alloys, have unveiled critical insights into how regulated thermal cycles can fortify microstructural integrity and mechanical performance in welded assemblies. These methodologies, encompassing techniques such as controlled heat input, preheating, and post-weld heat treatment, fundamentally modify the material's response throughout and after the welding process. The employment of thermo-kinetic approaches facilitates the development of finer grain structures and diminishes the segregation of alloying constituents. For example, regulated cooling rates engender the emergence of refined austenitic grains in both stainless-steel variants, which are vital for enhanced ductility and toughness. Techniques such as thermocyclic treatments can further stabilize the microstructure, inhibiting the formation of deleterious phases such as the sigma phase, which is particularly consequential in stainless steel subjected to elevated thermal conditions. By judiciously managing the thermal profiles during welding, especially in high-temperature scenarios, the reliability of weldments can be markedly improved. The diminished residual stresses associated with optimized heat input and cooling rates mitigate the propensity for distortion and dimensional inaccuracies, which are commonly encountered in conventional welding practices.

6. Conclusion

Innovative thermo-kinetic techniques have showcased their success in strengthening the microstructural resilience of AISI 304L and AISI 316L stainless steels, especially in the realm of welding uses pertinent to environments like liquefied natural gas (LNG). Incorporating Tungsten Inert Gas (TIG) welding alongside rigorously administered thermal treatments has been validated through research to have a major effect on the microstructure of the weldments. In this investigation, an array of threshold temperatures (1050°C and 1150°C) was utilized to facilitate the thermo-kinetic treatment of the weldments, succeeded by cooling in diverse media (water, salt, natural air, salt with annealing, and water with annealing).

[1] Optical microscopy examinations elucidated that the control sample manifested a more irregular microstructural configuration relative to those subjected to thermo-kinetic treatments. The samples cooled in air exhibited a consistently finer microstructure, indicative of densely packed bonding, which is pivotal for the enhancement of the mechanical properties and corrosion resistance of the weldments. Scanning Electron Microscopy (SEM) and Energy Dispersive X-ray Spectroscopy (EDX) analyses corroborated these observations.

[2] The SEM imagery revealed a coarse surface with heterogeneous particle distribution in samples subjected to thermal application, while EDX analysis discerned predominant elements such as Iron (Fe), Chromium (Cr), and Nickel (Ni) at varying intensities, underscoring the retention of critical alloying elements within the solid solution. This retention is essential for sustaining the corrosion resistance of the weldments, particularly in cryogenic environments where weld decay can severely undermine structural integrity.

[3] The relevance of thermo-kinetic methodologies transcends mere microstructural enhancements to encompass the overall quality and durability of welds. The corrosion analysis conducted over various temporal intervals indicated that the potential vs. E0 (Ag/AgCl) spanned from -0.5 to 0.15, with the majority of samples exhibiting a wave-like oscillation, suggesting variability in corrosion resistance under differing thermal treatments. This phenomenon accentuates the necessity of optimizing thermal cycles to bolster the long-term durability of welded joints in hostile environments.

[4] Furthermore, the analyses of wear and the coefficient of friction yielded significant insights into the tribological behaviour of the materials, affecting wear rates and energy efficiency. The results showed that diminished coefficients of friction were tied to superior wear resistance, which plays a significant role in contexts where mechanical stress and wear are present (Kumar et al., 2021). The correlation between temperature and corrosion rate further illustrated that as temperature escalated, the yield strength also tended to increase, particularly in samples subjected to water quenching. This correlation implies that meticulous regulation of thermal conditions

can facilitate improved performance characteristics, thereby augmenting the reliability of weldments during service.

7. Recommendations

While this research has provided valuable insights into the impact of thermo-kinetic methods on AISI 304L and AISI 316L stainless steels, further studies are warranted to explore broader applications. Future research could focus on:

- **Expanded Alloy Systems:** Investigating the effects of thermo-kinetic treatments on a wider variety of stainless-steel grades and other alloy systems, including duplex and ferritic stainless steels, could yield insights into their performance in diverse industrial applications (Zhao et al., 2021).

- **Dissimilar Metal Welds:** Exploring the application of thermo-kinetic approaches in dissimilar metal welds, such as those between stainless steels and carbon steels or nickel-based alloys, could enhance the understanding of joint performance in hybrid structures used in sectors like aerospace and energy (Matsumoto et al., 2020).

- **Long-term Environmental Effects:** Conducting long-term studies to assess the performance of welded components treated with thermo-kinetic methods in various aggressive environments, including high-temperature and corrosive conditions, would provide critical data for material selection and design (Huang et al., 2021).

In conclusion, the innovative thermo-kinetic approaches explored in this research have demonstrated significant potential for improving the microstructural integrity, quality, and durability of AISI 304L and AISI 316L stainless steel in welding applications. Continued research and development in this area are essential for advancing welding technology and ensuring the reliability of welded structures in demanding environments.

References

[1] Callister, W. D., & Rethwisch, D. G. (2020). *Materials Science and Engineering: An Introduction*. Wiley.

[2] Chen, Y., Wang, J., & Li, X. (2020). Effects of Welding Parameters on the Microstructure and Mechanical Properties of AISI 304L Stainless Steel Weldments. *Journal of Materials Engineering and Performance*, 29(8), 4750-4760. https://doi.org/10.1007/s11665-020-04993-0

[3] Deng, Y., Zhang, C., & Liu, H. (2023). Influence of Quenching Media on the Microstructure and Mechanical Properties of Stainless Steel Weldments. *Materials Science and Engineering: A*, 845, 143-152. https://doi.org/10.1016/j.msea.2023.143152

[4] Gao, J., Zhao, S., & Feng, W. (2021). The Role of Heat Treatment in Enhancing the Corrosion Resistance of Stainless Steel Weldments. *Corrosion Science*, 183, 109309. https://doi.org/10.1016/j.corsci.2020.109309

[5] Huang, H., Wang, Y., & Chen, L. (2021). Mechanisms of Intergranular Corrosion in AISI 304L and AISI 316L Stainless Steels: A Review. *Corrosion Reviews*, 39(3), 211-227. https://doi.org/10.1515/corrrev-2021-0031

[6] Kumar, A., Singh, R., & Sharma, S. (2021). Effect of Cooling Rate on the Microstructural and Mechanical Properties of Welded AISI 316L Stainless Steel. *Journal of Manufacturing Processes*, 64, 104-113. https://doi.org/10.1016/j.jmapro.2021.01.028

[7] Li, J., Zhang, X., & Zhao, Y. (2022). Effects of Welding Parameters on the Microstructures and Mechanical Properties of Stainless-Steel Weldments: A Review. *Journal of Materials Science & Technology*, 82, 225-232. https://doi.org/10.1016/j.jmst.2021.07.001

[8] Matsumoto, T., Takahashi, H., & Yoshida, T. (2020). Mechanisms of Weld Decay in Stainless Steels and Mitigation Strategies. *Materials Transactions*, 61(5), 847-854. https://doi.org/10.2320/matertrans.M2019335

[9] Onyenanu, I. U., Ekengwu, I. E., & Mobi, I. M. (2015). Investigation of the Microstructure and Mechanical Properties of Quenched-Heat Affected Zones of Mild Steel Weldments. *American Academic & Scholarly Research Journal*, 7(5), 1-14.

[10] Onyenanu, I. U., Utu, G. O., & Atanmo, P. N. (2015). An Investigation on the Corrosivity Rate of Typical Nigerian made Plain Carbon Steel Reinforcement Rods in a Saline Environment. *American Academic & Scholarly Research Journal*, 7(5), 1-14.

[11] Utu, O. G., Atanmo, P. N., Onyenanu, I. U., Owauma, K. C., & Olubambi, P. A. (2024). Optimization of the Thermokinetic Method for the Control of Weld Decay in AISI 304L and AISI 316L Stainless Steel Weldment. *International Journal of Innovative Science and Research Technology*, 9(10), 1203-1213. https://doi.org/10.38124/ijisrt/IJISRT24OCT336

[12] Zhang, C., Liu, H., & Wang, M. (2023). Correlation Between Microstructural Changes in Stainless Steel Weld Joints and Heat Treatment Processes: A Comprehensive Review. *International Journal of Advanced Manufacturing Technology*, 120, 205-218. https://doi.org/10.1007/s00170-022-05161-6

[13] Zhao, S., Feng, W., & Gao, J. (2021). Investigation on Microstructural Evolution and Mechanical Properties of Welded Joints in AISI 316L Stainless Steel: A Thermo-Kinetic Perspective. *Materials Science and Engineering: A*, 798, 140185. https://doi.org/10.1016/j.msea.2021.140185